Available online at www.sciencedirect.com
SCIENCE DIRECT
Journal of Physics and Chemistry of Solids 67 (2006) 896–902
JOURNAL OF PHYSICS AND CHEMISTRY OF SOLIDS
www.elsevier.com/locate/jpcs

One-dimensional nanomaterials of vanadium and molybdenum oxides

Wen Chen *, Liqiang Mai, Yanyuan Qi, Ying Dai

Institute of Materials Science and Engineering, Wuhan University of Technology, Wuhan 430070, People's Republic of China

Abstract

One-dimensional vanadium and molybdenum oxide nanomaterials have been synthesized using a rheological reaction followed by a self-assembling process. The replacement of V in VONTs by Mo with a larger ionic radius results in a shorten diffusion length of Li^+ ions and an improved electrochemical performance. The special composites composed of nano-scale Ag and organic template molecular exist in the hollow nanotubes and between the VO_x layers of nanotube wall resulting in the change of the interlayer distance of nanotube wall and nanotube diameters, and thereby, improved electrochemical performance. The VO_2 (*B*) nanorods were treated by H_2O_2 and CTAB solution and VO_2 (*M*) nanorods were attained through phase transfer process of $VO_2(B) \rightarrow VO_2(R) \rightarrow VO_2(M)$. The observed MoO_3 nanorods with the average width of 100 nm consist of several thin layers contacting each other. The electrochemical property of this special structure is proved to be good.

Keywords: A. Nanostructures; A. Oxides; B. Chemical synthesis; D. Electrochemical properties

1. Introduction

The discovery of carbon nanotubes (CNTs) in 1991 has urged the naissance of more and more one-dimensional (1D) nanostructure materials, such as nanotubes, nanowires and nanorods due to their remarkable physicochemical properties and their great potential for nanodevices [1–6]. The outstanding structural versatility of the intercalation compounds such as vanadium oxides, molybdenum oxides and their derivatives has been receiving significant attention especially with respect to applications in catalysis and as electrochemical devices [7–10]. The fabrication of vanadium and molybdenum oxide material in nanostructured form and with anisotropic morphology appears to be a particularly attractive goal. The ongoing success on all frontiers of nanomaterials research makes it more and more difficult to keep up to date with all new achievements and to derive general trends that could be the main pathways to future technology. Even a short scan of novel publications concerning these topics clearly reveals that hydrothermal self-assembling synthesis is one of the most powerful tools providing access to distinct morphologies of nanomaterials. In this paper we will discuss the control or modification of the structure of vanadium and molybdenum oxide nanomaterials, and thereby their properties, by the tailored control of the synthesis conditions. Selected recent examples from our laboratory illustrate the straightforward applicability of this strategy upon the production of both nanotubes and nanorods that are uniformly and quantitatively produced combining the rheological reaction and hydrothermal self-assembling process.

2. Experimental

The methods used were similar to those reported earlier [6,11]. Thus, oxides normally in their highest oxidation state were mixed in aqueous media together with an organic templating agent such as the hexadecylamine and cetyltrimethyl ammonium bromide (CTAB) and the mixture stirred for 48 hours in air. The resulting rheological suspension was transferred into a Teflon-lined autoclave with a stainless steel shell. The autoclave was kept at 180 °C for about a week. The final product was washed with distilled water and dried at 80 °C for 8 h.

XRD experiments were done on a D/MAX-III X-ray diffractrometer with Cu Kα radiation and graphite monochrometer. SEM images were attained using a JSM-5610LV scanning electron microscope at 20 kV. HRTEM images were taken in a JEOL JEM-2010FEF microscope operated at 200 kV. XPS measurements were carried out by using an ESCALAB MKII multi-technique electron spectrometer. AFM images were captured using NanoScope IV scanning probe microscope in tapping mode operation. Redox titration was conducted to determine the homogeneity of the Mo repartition as previously described [18]. HP-4294A apparatus and self-designed heating instrument were used to investigate the

* Corresponding author. Tel.: +86 27 87651107; fax: +86 27 87864580.
E-mail address: chenw@mail.whut.edu.cn (W. Chen).

0022-3697/$ - see front matter © 2006 Elsevier Ltd. All rights reserved.
doi:10.1016/j.jpcs.2006.01.074

electrical properties of the samples. The cathode preparation and the test cell were similar to as described previously [5,11]. Li metal was used as the anode. The test cells containing 1 M $LiPF_6$-EC-DEC (1:1 volume ratio) were usually charged to 3.9 V and discharged to 1.4 V at a 0.15 °C rate. The experimental accuracy in the discharge capacity measurements is ± 1 mAh/g.

3. Results and discussion

3.1. Modification of vanadium oxide nanotubes

Selective doping of nanotubes is a promising route for further development of new curved nanomaterials. The first attempt was made [11,12] to prepare Mo-doped vanadium oxide nanotubes via a rheological phase reaction followed by a self-assembling process. It should be emphasized that when the doping is in the range of about 0–10 mol% the morphology and structure of undoped and doped nanotubes appear as a whole similar, and the differences concern inter-wall distances between oxide walls and some electrochemical properties. Titration technique and XPS measurement have been done to confirm the success of Mo doping and the homogeneity of the Mo repartition and the results show that the content of Mo is very near to its primary doping level of Mo (1 mol%). In contrast with the undoped sample, there is a noticeable shift of the 001 peak toward lower diffraction angle for the Mo doped sample corresponding to increase of the interlayer distance from 3.35 to 3.40 nm (Fig. 1A). The change of the interlayer distance is also confirmed by the ED result. Meanwhile, it can be found that *a* in 2D tetragonal cell increases from 0.615 to 0.623 nm [8]. The changes for interlayer distance and *a* can also be attributed to the replacement of V in vanadium oxide nanotubes by Mo with a larger ionic radius. Interestingly, heat treatment results in drastic reduction of the interlayer distance to 1.55 nm which is clearly due to the removal of organic template between oxide layers in the nanotubes. The *hk0* reflections due to the vanadium oxide sheets remain at the same positions showing that the structure of the layers remains the same. The interlayer distance between oxide layers in the $(V_{0.99}Mo_{0.01})_x$ONTs increases owing to replacement of some V in nanotubes by Mo, resulting in a shorten diffusion length of Li^+ ions and an improved electrochemical performance (Fig. 1B). Moreover, the electrochemical performance of $(V_{0.99}Mo_{0.01})_x$ONTs is further enhanced by removing the residual organic template by heating in an inert atmosphere [11].

Ag-modified VONTs (Fig. 2) were also prepared by adding Ag_2O to the V_2O_5 as the starting materials. In comparison with the pure VONTs, the Ag-containing nanotubes have shorter lengths (0.5–2 μm), a wider average outer diameter (70–110 nm) and a narrower inner diameter (10–30 nm)(Fig. 2A–C)). Interestingly, HRTEM images for the areas in the hollow tubes and between the VO_x layers of nanotube wall shows an obvious fringe with a regular spacing of ~0.23 nm) (see the inset of Fig. 2C), which is quite close to the inter-plane distance of (111) for Ag. EDS measurement confirms the metallic Ag composition (Fig. 2D). Here, the results may indicate that the Ag is present in the hollow tubes and between the VO_x layers of nanotube wall. Such features were not observed for other kinds of cation-exchanged or cation-doped VO_x nanotubes [8,11,13]. The diffraction peaks of Ag are found in the XRD pattern of Ag-containing VONTs(Fig. 3A(b)). And in contrast with the pure sample, there is a noticeable shift of the 001 peak toward higher diffraction angle for the Ag-containing sample corresponding to increase of the interlayer distance from 3.35 nm to 4.09 nm. The result suggests that Ag nanocrystals are dispersed in organic template molecular via certain interaction with the latter. Such composites composed of nano-scale Ag and organic template molecular exit in the hollow nanotubes and between the VO_x layers of nanotube wall, resulting in the increase of the interlayer distance of nanotube wall and change of nanotube diameters [11,13], which is in good agreement with the above TEM analysis.

In contrast with the pristine V_2O_5 showing distinctive plateaus due to structural changes [14], the potentials decrease more smoothly down to ~2.0 V for both nanotube

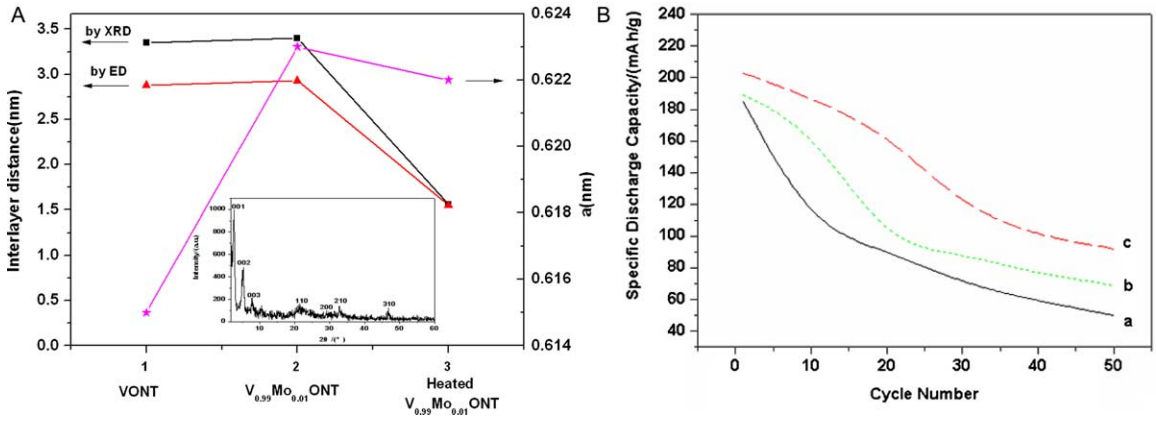

Fig. 1. (A) interlayer distance and *a* value of VONT, $V_{0.99}Mo_{0.01}$ONT and heated $V_{0.99}Mo_{0.01}$ONT (The inset shows the XRD pattern of as-synthesized VONT); (B) the specific discharge capacity of VONT (a), $V_{0.99}Mo_{0.01}$ONT (b) and heated $V_{0.99}Mo_{0.01}$ONT (c) Note: ?The estimated error in the calculated *a* is 1.8%. ?This deviation of the layer distance according to ED and XRD data is ascribed to partial rearrangement of the flexible, paraffin-like arrangement of template molecules between the layers under the influence of the electron beam and to an occasional loss of template molecules under the high vacuum conditions.

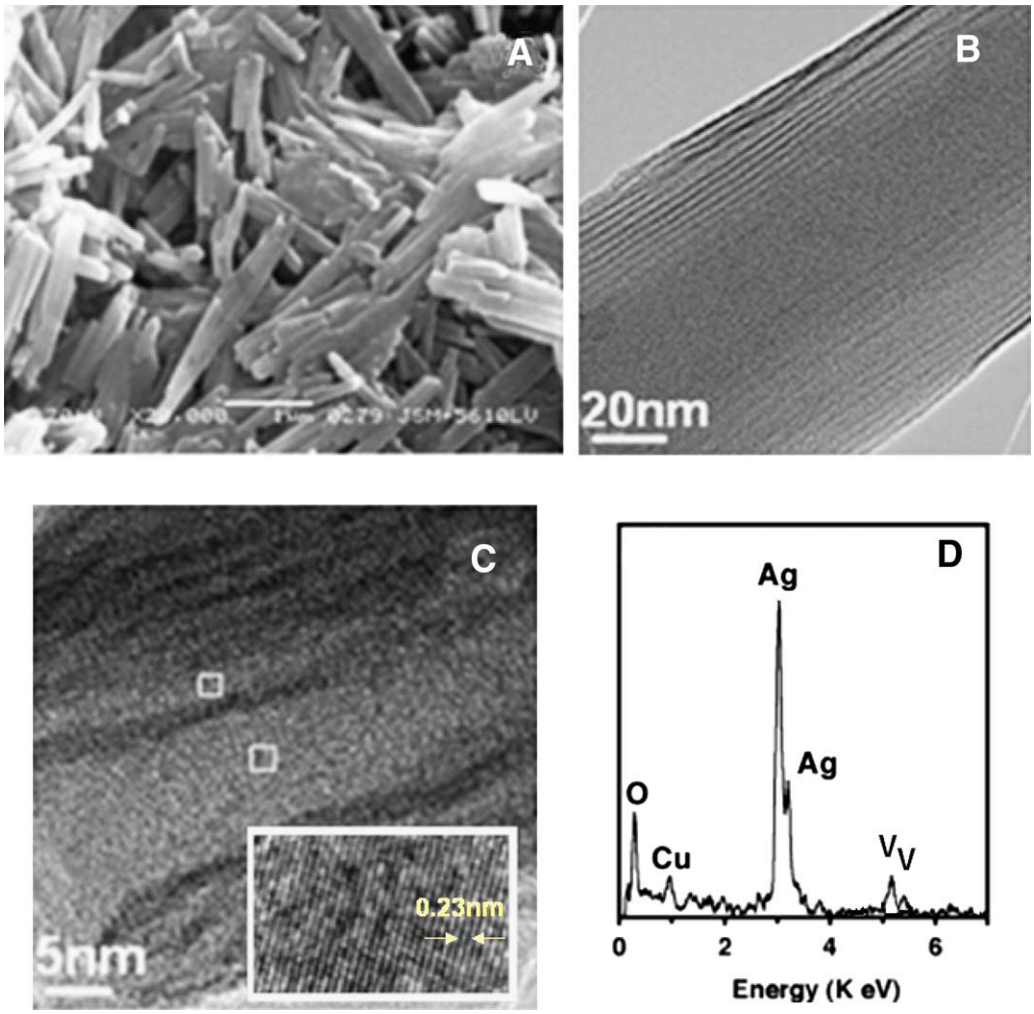

Fig. 2. SEM (A), TEM (B,C) images and EDS spectrum of the Ag-containing VONTs (the inset in Fig. 2C shows the lattice fringe of selected area).

samples(Fig. 3B). Similar continuous decrease in potential has been also observed for V_2O_5 xerogel [15] and conductive polymer/V_2O_5 xerogel hybrids [16], of which common structural feature is the separation of vanadium oxide layers owing to the presence of interlayer molecules. The disturbed layer stacking derived by the change of interlayer distance would make structural disorders, e.g. reduced covalency of bondings between some vanadium and oxygen atoms, which thereby creates empty sub-bandgap V^{5+}:$3d^0$ energy states rather uniformly distributed between 3.7 and 2.0 V [11].

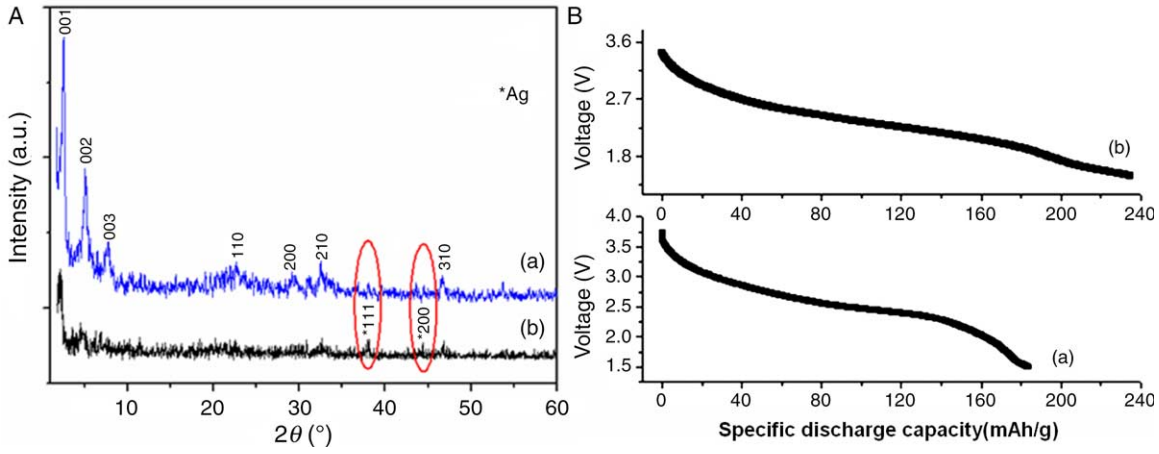

Fig. 3. XRD patterns of the pure (a) and Ag-containing (b) VONTs (A); First discharge cure of pure (a) and Ag-containing (b) VONTs(B).

It is noted that the first discharge capacity of Ag-containing VONTs (234 mAh/g) is higher than that of the pure VONTs (185 mAh/g). Meanwhile, the former exhibits better cycling properties than the latter. Furthermore, the conductivity is at a magnitude of 10^{-7} S/cm for pure VONTs and 10^{-5} S/cm for Ag-VONT sample. After being modifying by Ag_2O, the electrical conductivity of vanadium oxide nanotubes increases by 2 orders of magnitude. According to thermal analysis, the tubular morphology for the Ag-VONTs is totally destroyed before 505 °C while the corresponding temperature for the pure VONTs is 300 °C, which indicates that the thermal stability is improved by introduction of Ag. Therefore, the improved electrochemical performance of the Ag-containing VONTs is assumed to be due to a higher electrical conductivity, better thermal stability and the increase of the VO_x interlayer distance because of introduction of Ag [17].

In addition, the structure and property of VONTs can be modified and improved by PEO intercalation, and copper or rare earth doping [23]. Therefore, it can be concluded that selective doping, polymer intercalation and non-doping introduction of other elements offer an effective pathway to stabilize structure of vanadium oxide nanotubes and improve their properties resulting in the applications in catalysis, sensors and as electrochemical devices.

3.2. Phase transition of VO_2 nanorods

It belongs to interesting research fields to prepare 1D nanomaterials of VO_2 and study their phase transition. The diffraction peaks (Fig. 4A) of the samples prepared via the rheological self-assembling method from V_2O_5 and CTAB can be indexed to VO_2 (B) phase consisted with the standard value of JCPDS 31-1438 (C2/m, $a=1.203$ nm, $b=0.3693$ nm, $c=0.642$ nm, $\beta=106.6°$) as well as minor V_6O_{13}. Compared with the standard data, the (110) peak is relatively strong which may be caused by the orientation growth of VO_2 (B). SEM and TEM images (Fig. 5A and B) show that the sample consists of straight nanorods with uniform diameters in the range 40–60 nm, and lengths ranging from 1–2 μm. The aspect ratio of the corresponding nanorods lies in the range of 25–40. Lengths and diameters of the nanorods depend on the conditions of the preparation, such as different template molecules, concentration and reaction time.

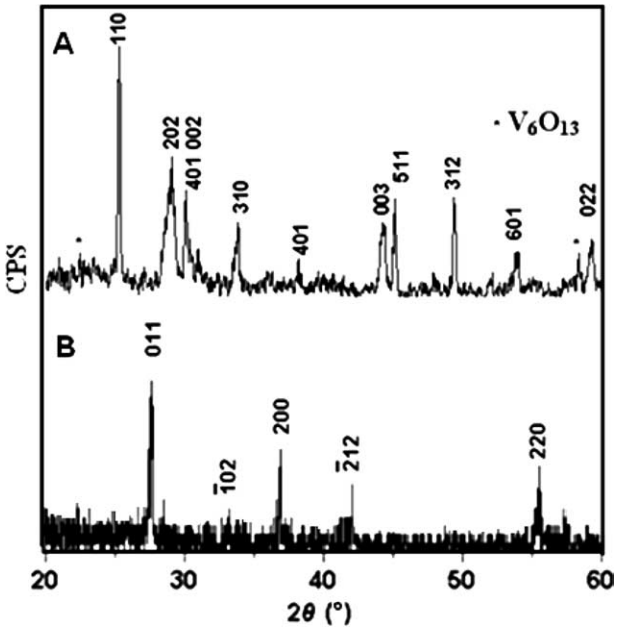

Fig. 4. XRD patterns of VO_2(B) (A) and VO_2(M) (B) nanorods.

In order to attain thermochromic VO_2 (M) nanorods, H_2O_2 and CTAB solution were used to treat the as-synthesized VO_2 (B) nanorods. XRD investigation confirms the success of the phase transfer of VO_2 nanorods. The XRD pattern of the sample after treatment is consistent with that of VO_2 (M) phase ($P2_1/a$, $a=5.744$ Å, $b=4.517$ Å, $c=5.376$ Å, $\beta=122.7°$) (Fig. 4B). Examination by SEM and TEM (Fig. 5C and D) shows that VO_2 nanorods with an approximate diameter of 100 nm and an average length of 1.5 μm are formed, which exhibits an interesting morphological feature: high magnification TEM micrographs reveal that they indeed form bundles of agglomerated smaller filaments with diameters ranging from 20 to 40 nm besides single nanorod. This interesting shape in the nanoscale dimension leads to the exposure of a large fraction of the atoms to the surface, making these materials promising candidates for the development of new functionalized materials.

The formation mechanism of VO_2 (B) nanorods can be interpreted as follows: in the formation of VO_2 (B) nanorods, CTAB plays a key role. CTAB is generally used as structure-directing template in the synthesis of 1D nanostuctured materials. Some literatures have reported that CTAB could reduce some inorganic materials with high redox activity, such as $KMnO_4$ and PbO_2 [19,20]. Similar to the synthetic procedure of $Li_xV_{2-\delta}O_{4-\delta}\cdot H_2O$ started from V_2O_5 and tetramethyl ammonium, which forms $[N(CH_3)_4]V_4O_{10}$ phase [21], we assume that CTAB acts as a ligand which coordinates with central vanadium to form the possible $[C_{16}H_{33}N(CH_3)_3]V_4O_{10}$ complex [18]. These complexes are then reduced to form VO_2 particles under hydrothermal condition. Small amount of B phase VO_2 particles serve as seeds for further growth. With the presence of CTAB, which could form rod-like micelle easily in solution, the VO_2 (B) phase slowly grow along the surface of CTAB micelle through a solid-solution-solid transformation progress and finally become nanorods. In order to testify the crucial effect of CTAB, some other surfactant or reductants were used such as hexadecylamine, ethylenediamine, and hydrazine monohydrate, but no B phase VO_2 was observed when other reaction conditions remained.

The phase transition of VO_2 nanorods from B phase to M phase is remarkable and very unusual. Generally speaking, the structures of the four VO_2 polymorphs, $VO_2(R)$, $VO_2(M)$, $VO_2(B)$, and $VO_2(A)$, are based on an oxygen bcc lattice with vanadium in the octahedral sites, the oxygen octahedra being more or less regular. They can be separated in two groups, depending on the mutual orientation of the fourfold axis of the

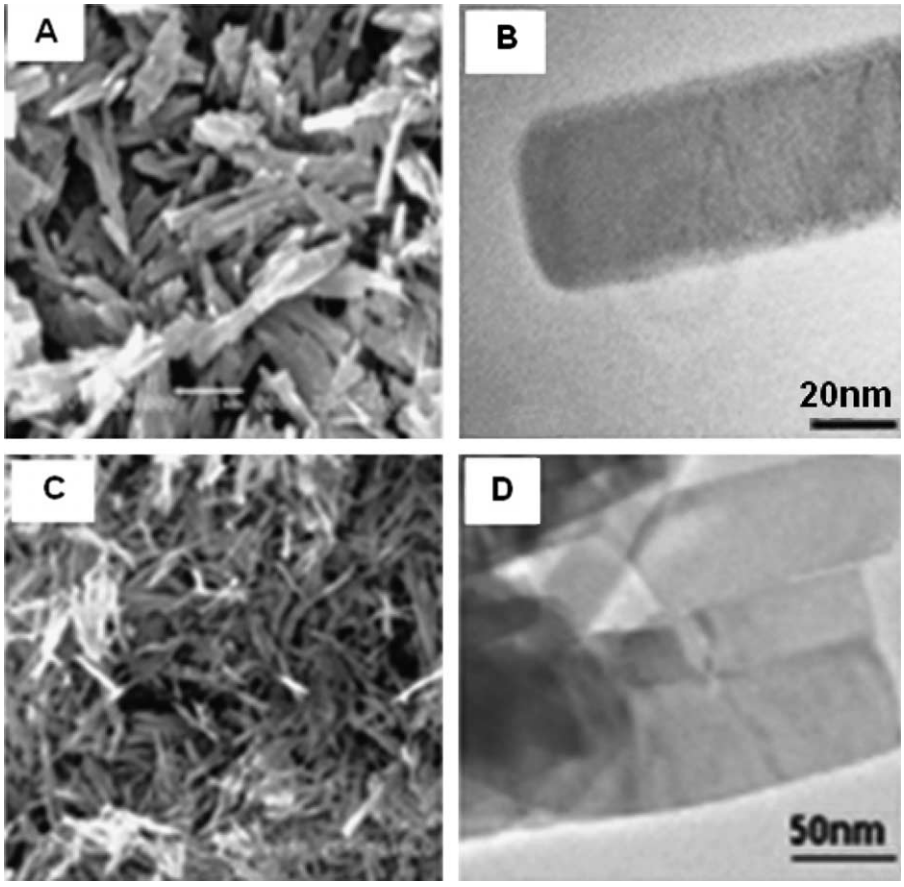

Fig. 5. Electronic microscopic images of $VO_2(B)$ nanorods (A, B) and $VO_2(M)$ nanorods (C, D).

oxygen octahedra. The oxygen octahedra can be aligned either along two perpendicular directions, as it is the case in rutile structure $VO_2(R)$, and in monoclinic deformed $VO_2(M)$; or oxygen octahedra can be mainly aligned along one direction as in $VO_2(B)$ and $VO_2(A)$. Note that these two groups correspond to two different values for the density. It is clear that, although these VO_2 polymorphs correspond to the same stoichiometry, their structures are very different. The most stable structure for vanadium dioxide is the so-called rutile structure $VO_2(R)$, which is stable from 68 to 1540 °C: the space group is $P4_2/mmm$ which gives rise to a very symmetric structure. The formation at 68 °C of the monoclinic $VO_2(M)$ is related to the appearance of a pairing between two V^{4+} along $\mathbf{c}_R$. The induced distortion leads to a lowering of the symmetry. The two other polymorphs of VO_2 have little in common with the rutile phase. They have larger cells, with octahedra mainly aligned along one crystallographic direction. The VO_2(B) structure can be considered as formed by two identical layers of atoms along **b**. Like V_6O_{13}, $VO_2(B)$ forms platelets. These platelets are preferentially oriented. They grow in (**a**,**b**) planes; in this plane one forms a network of corner sharing octahedra.

The following is about phase transition of VO_2 nanorods. When H_2O_2 was added into the suspension of $VO_2(B)$ nanorods, a vast amount gas (O_2) and heat were released. By heating up the $VO_2(B)$, this structure changes into a structure of higher symmetry, more stable from a thermodynamical point of view. This change includes a translation of the planes perpendicular to the bcc *c* axis, back to their position in the parent phase, giving rise to an intermediate structure with an angle different from 90°. Further heating disorders even more the vacancies and the vanadium atoms on the octahedral sites. When complete disorder is reached, the crystal assumes the more stable rutile structure. When they are allowed to cool to room temperature, a phase transition at approximately 68 °C from *R* phase to *M* phase occurs. Obviously, the use of CTAB is helpful to keep nanorod shape and structure. More research need be done to testify our above explanation.

Moreover, the charge/discharge voltage plateau for the VO_2 (*B*) nanorods is 2.75/2.5 V, and the specific charge and discharge capacity are 254 and 247 mAh/g, respectively. The first cycle efficiency exceeds 97.5%. The discharge specific capacity arrives at 180 mAh/g after 30 cycle(Fig. 6A). In contrast to normal VO_2 crystal material whose reversible capacity is about 160 mAh/g, VO_2 nanorods possess better electrochemical property which is due to stable structure and high surface activity [18]. For the VO_2 (*M*) nanorods, there is an obvious phase transition at $T_c = 65$ °C. In the transition process, the resistivity increases sharply (Fig. 6B). And the activation energy of $VO_2(M)$ nanorods is 0.2 eV by calculation, and the Fermi energy band is at about the middle of forbidden band which account for good crystallization [22].

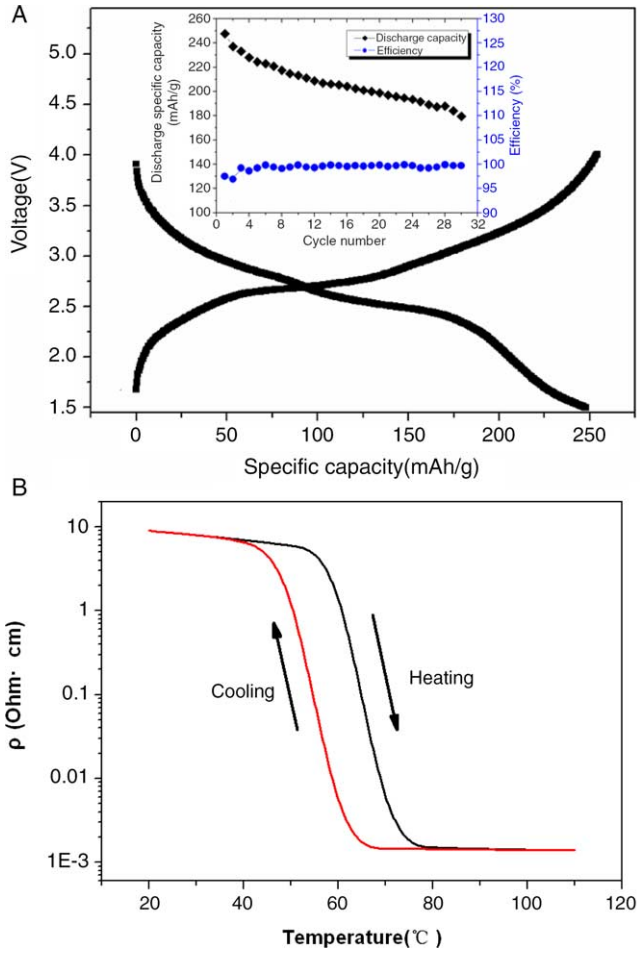

Fig. 6. (A)initial charge/discharge curve of VO_2 (*B*) nanorods(the inset is the curves of their specific capacity and efficiency vs. cycle number); (B)electrical property of VO_2(*M*) nanorods.

3.3. Controlled formation of MoO_3 nanorods

Due to the size effect and quantum confinement effect, 1D MoO_3 nanomaterials are becoming more and more important and necessary. XRD investigation confirms that the as-synthesized sample is MoO_3. All diffraction peaks can be indexed to the MoO_3 phase consistent with the standard value of JCPDS No.05-0508, and the strong intensity of reflection peaks of (020) and (040) indicate the anisotropic growth.

The diameters of the nanorods are between 60 and 150 nm and their length lies between 1 and 6 μm. And the corresponding SAED pattern shows that the nanorod is single crystalline with the [001] direction parallel to the rod axis (inset in Fig. 7A). All nanorods exhibit the [001] direction for the rod axis. The surface topography of the nanomaterials was also studied by AFM (Fig. 7B). It is interesting to note that several thin layers connect each other to form the so-called nanorods. And the special structure can provide more electrolyte-filled channels between the layers for faster transport of the ions to the insertion sites, which is helpful to improve their electrochemistry performance. Battery testing shows that MoO_3 nanorods exhibit a total reversible capacity of about 300mAh/g in the potential range from 3.25 to 1.5 V. There is a voltage plateau around 2.75 V, along with a shoulder around 2.3 V. After 5 cycles, the specific discharge capacity is 266 mAh/g (Fig. 8). For bulk MoO_3, however, the first discharge capacity is 254mAh/g and the cycle property is poor. We propose that good electrochemical performance of MoO_3 nanorods is attributed to their special layered structure.

Although the formation mechanism of the MoO_3 nanorods stays an open question, it is obvious that the special structure of MoO_3 sol plays an important role in the reaction. MoO_3 is known as a typical 2D layered structure consisting of double layers of edge- and vertex-sharing MoO_6 octahedra being weakly held together by Van Der Waals bonds. And these layers can be propped open by intercalated guest molecule. H_2O molecule is intercalated between the MoO_6 octahedron layers in the MoO_3 sols and the layers form thin nanobelts which connect with each other resulting in the formation of the observed nanorods in the suitable temperature and pressure [23]. It is obvious that the forming mechanism of the nanorods in this paper is different from that previously reported [24]

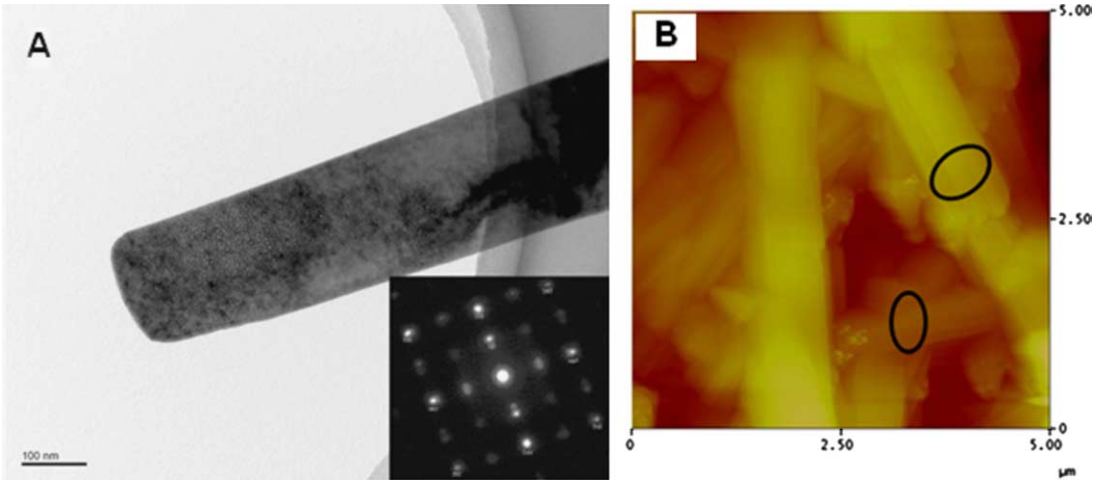

Fig. 7. TEM (A) and AFM (B) images of MoO_3 nanorods.

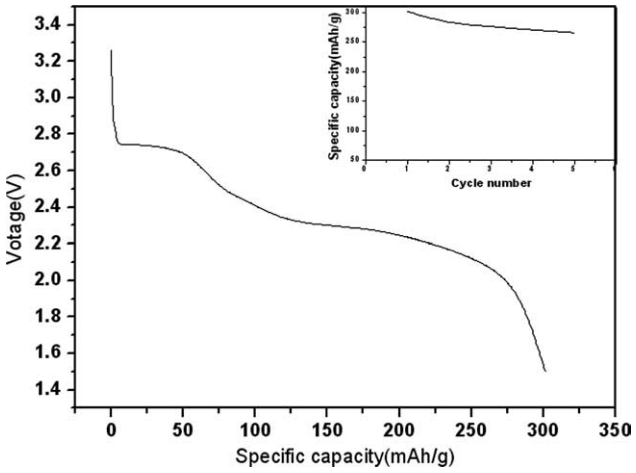

Fig. 8. First discharge cure of MoO_3 nanorods (the inset is cycle performance).

where the fibrous molybdenum oxide was obtained via the intercalation of primary amines into the layered structure of molybdenum acid and subsequent transformation of the lamellar molybdenum oxide-amine intermediate into the fibrous products. In addition, the nanorods can not be obtained by the MoO_3 powders in replace of their sol in the same reaction condition. This further confirms the above mechanism.

4. Summary and outlook

The discovery of the carbon nanotubes has catalyzed a fruitful and still growing interest in nanotubes and nanorods, both in application-oriented industrial as well as in basic research. Although carbon nanotubes are still the most widely investigated examples for 1D nanomaterials, the world-wide search in other systems is steadily increasing this structural family. This growing diversity is not only because of an extension of the systems investigated but also to the skillful application of a wide range of different synthetic methods. Interesting and effective among them are rheological self-assembling routes that involve rheological reactions followed by hydrothermal self-assembing process with template-directed or template-free methods. Controlled formation and modification of anisotropic materials, such as, nanotubes and nanorods provide the interesting physical and chemical properties which quite often differ from those of the corresponding bulk materials and those of isotropic nanoparticles. The usefulness of these properties for the electrochemical application is mentioned in this paper. However, it must be stated that this is only the beginning. Because of ongoing attempts to further miniaturize electronic, optical, and mechanical components, there is a need for materials that could be used as building blocks in the size region of a few nanometers. Considering these perspectives, we are sure that the role of nanotubes and nanorods in a future nanotechnology can hardly be overestimated.

Acknowledgements

This work was supported by the National Natural Science Foundation of China (Grant No. 50372046), the Key Project of Chinese Ministry of Education (Grant No. 104207), Nippon Sheet Glass Foundation for Materials Science and Engineering (2005) and the Teaching and Research Award Program for Outstanding Young Professors in Higher Education Institute, MOE, People's Republic of China.

References

[1] S. Iijima, Nature 354 (1991) 56.
[2] A.M. Morales, C.M. Lieber, Science 279 (1998) 208.
[3] P.M. Ajayan, O. Stephan, P. Redlich, C. Colliex, Nature 375 (1995) 564.
[4] M.E. Spahr, P. Bitterli, R. Nesper, M. Muller, F. Krumeich, H.U. Nissen, Angew. Chem. 110 (1998) 1339.
[5] M. Niederberger, F. Krumeich, H.J. Muhr, M. Muller, R. Nesper, J. Mater. Chem. 11 (2001) 1941.
[6] L.Q. Mai, W. Chen, Q. Xu, Q.Y. Zhu, C.H. Han, J.F. Peng, Solid State Commun. 126 (2003) 541.
[7] W. Chen, Q. Xu, Y.S. Hu, L.Q. Mai, Q.Y. Zhu, J. Mater. Chem. 12 (2002) 1926.
[8] A. Dobley, K. Ngala, S. Yang, P.Y. Zavalij, M.S. Whittingham, Chem. Mater. 13 (2001) 4382.
[9] L.P. Tian, W.Sh. Li, H. Li, Mod. Chem. Ind. 20 (2000) 19.
[10] G.T. Chandrappa, N. Steunou, S. Cassaignon, C. Bauvais, P.K. Bisas, J. Livage, J. Sol–Gel. Sci. Technol. 26 (2003) 593.
[11] L.Q. Mai, W. Chen, Q. Xu, J.F. Peng, Q.Y. Zhu, Chem. Phys. Lett. 382 (2003) 307.
[12] A.N. Enyashin, V.V. Ivanovskaya, Y.N. Makurin, V.L. Volkov, A.L. Ivanovskii, Chem. Phys. Lett. 392 (2004) 555.
[13] F. Krumeich, H.-J. Muhr, M. Niederberger, F. Bieri, R. Nesper, Z. Anorg, Allg. Chem. 626 (2000) 2208.
[14] J.M. Cocciantelli, M. Menetrier, C. Delmas, J.P. Doumerc, M. Pouchard, M. Broussely, J. Labat, Solid State Ionics 78 (1995) 143.
[15] H.K. Park, W.H. Smyrl, J. Electrochem. Soc. 141 (1994) L25.
[16] G.R. Goward, F. Leroux, L.F. Nazar, Electrochim. Acta 43 (1998) 1307.
[17] C.W. Kwon, A. Poquet, S. Mornet, G. Campet, J. Portier, J.H. Choy, Electrochem. Commun. 4 (2002) 197.
[18] L.Q. Mai, Dissertation for PhD, Wuhan University of Technology, China, 2004.
[19] S. Ching, J.L. Roark, N.G. Duan, S.L. Suib, Chem. Mater. 9 (1997) 750.
[20] M.H. Cao, C.W. Hu, G. Peng, Y.J. Qi, E.B. Wang, J. Am. Chem. Soc. 125 (2003) 4982.
[21] A.M. Kannan, A. Manthiram, Solid State Ionics 159 (2003) 265.
[22] L.Q. Mai, W. Chen, Q. Xu, J.F. Peng, Q.Y. Zhu, H. Yu, Rare Metal. Mater. Eng. 32 (2003) 748.
[23] X.C. Wu, Y.R. Tao, L. Dong, J.M. Hong, J. Mater. Chem. 14 (2004) 901.
[24] M. Niederberger, F. Krumeich, H.J. Muhr, M. Muller, R. Nesper, J. Mater. Chem. 11 (2001) 1941.